



Jazan University

College of Engineering and Computer Sciences

Department of Mechanical Engineering

Research Collaboration Letter

October 10, 2025

From: Dr. Ayman M Alneamy

Associate Professor, Department of Mechanical Engineering

Jazan University, Saudi Arabia

To: Dr. Naveen Kumar A

Assistant Professor, Department of Mechanical Engineering

Siddharth Institute of Technology & Sciences, Narapally Village 500088, India

Dear Dr. Naveen Kumar A,

We are pleased to express our keen interest in establishing a formal research collaboration with the Mechanical Vibration Laboratory, Jazan University, through a **Memorandum of Understanding (MoU)**. Our institution actively promotes international academic partnerships aimed at advancing research and innovation across engineering disciplines.

This collaboration is intended to foster joint research initiatives and other academic activities. We believe that mutual cooperation between our research groups will strengthen both research capabilities and global academic excellence in the field of mechanical engineering, particularly in vibration analysis, structural dynamics, and composite materials.

We look forward to your positive response and a long-term partnership that will benefit both our research communities. Thank you for your consideration.

Dr. Ayman M Alneamy

Mechanical Vibration, Health Monitoring and System Dynamics Stability Expert

Department of Mechanical Engineering



Dynamic Stability Behavior Prediction of Initially Cracked Doubly Curved Laminated Composite Shell Structures—A Higher-Order FE Approach

Abhishek Kumar Sahu^{*,†,1}, Ashish Chakrabarti^{*,†,2}, Nageswari Kumar Akkavali^{†,3}
 and Vibashit Khatiwala^{†,4}

¹Department of Mechanical Engineering
 National Institute of Technology
 Rourkela, 769008, India

²Department of Mechanical Engineering
 Indian Institute of Technology
 Varanasi, Varanasi, 221005, India

³Induslakeshaperschoolofaerospacemgmt.com
 Mysorempur6470@gmail.com
⁴nageswari.kumar.akkavali@gmail.com
 vikhatiwala02@yahoo.com

[†]Nitin Sharma[©]
 School of Mechanical Engineering, MIT (Deemed to be University)
 Ghoshnagar, 751031, India
 nitn_tnn@gmail.com

[©]Lokesh Srivastava[©]
 Advanced Systems Laboratory, DRDO, Kanchan Bagh
 Hyderabad 500056, India
 lokeshsrivastava_ael@yahoo.in

[©]Sobhan Kumar Panda^{©**}
 Department of Mechanical Engineering
 National Institute of Technology Rourkela, 769008, India
 sskpanda@nita.ac.in; panda@nita.ac.in

Received 11 July 2025
 Accepted 23 September 2025
 Published

The current investigation explores the presence of cracks and their influence on the dynamic instability behavior of laminated composite curved (single/doubly) shell structures when subjected to in-plane loading. The numerical model is developed in a higher-order strain-displacement relation utilizing a nine-noded iso-parametric element.

^{**}Corresponding author.

2750078-1

A. N. Saba *et al.*

parameterizing time degrees of freedom per node. The mathematical model incorporates the crack type of damage to investigate the parametric excitation response. The final form of the equation of motion for a damaged layered structure is derived using Lagrange's equations under the parametric excitation. The instability zone and the eigenfrequencies are obtained by solving the Mathieu-type ordinary differential equations with a first-order approximation obtained through a Fourier series expansion. First, the non-independent behavior of the predicted numerical solution is verified and extended to check the model accuracy by comparing the results with published data. The frequency responses obtained using the derived computational are close to the reference data and the deviations are close to a value within the accepted range (±0.01%). Additionally, a few estimates are solved to evaluate the influence of variation of input design parameters on the final responses while the structure is under parametric excitation.

Keywords: Dynamic instability; damage; excitation; frequency; finite element method; higher-order kinematic model.

1. Introduction

The dynamic responses of the laminated composite have been investigated extensively using the available standard techniques and/or modified methodologies in the recent past to understand the stability behavior. In this regard, the behavior of laminated plates under the influence of any arbitrary dynamic loading on the cylindrical bending is analyzed,¹ focusing on correlation functions of displacement variances. In another research work, excitation was induced using electromagnetic devices, and instability regions were identified using analytical techniques.² Chiu and Lam³ developed a methodology to analyze the dynamic behavior of laminated composite plates subjected to low-velocity impact, utilizing second-order differential equations formulated through Lagrange's principle and Hertzian contact theory. Further exploration focused on various laminated composite structures, nonlinear oscillations, and disordered dynamics, including rectangular thin plates and beams. The finite element method (FEM) analysis transversely point-loaded composite cylindrical shells, addressing stability issues and nonlinear responses.⁴ The study efficiently identifies bifurcation points and establishes new benchmarks for asymmetric deformations and post-buckling regimes. Von Karman-type equations have been deployed to derive governing equations, with methods such as Galerkin and asymptotic perturbation revealing complex behavior like multi-pulse orbits and chaotic motion.⁵ Additionally, the investigation extended to dynamic stability under periodic loads, utilizing first-order shear deformation theory. Mathien, Hill-type differential equations determined instability regions, showcasing the significant influence of various parameters on instability.⁶ A study on the free vibration of delaminated/interact composite beams or sandwich plates has been presented employing FE or wavelet FE modeling alongside the harmonic balance method to assess bifurcation behavior and stability characteristics. The parametric instability of carbon nanotube (CNT)-reinforced composite cylindrical panels under thermal and periodic in-plane excitations has been evaluated utilizing Galerkin's and Bolotin's method, and the effects of CNT distribution, volume fraction, curvature,

2nd Reading

October 8, 2025 11:55 WSPC/165-IJSSD 2750078

Dynamic Stability Behavior Prediction

and pre-buckling on instability responses are examined,¹⁶ Pradyumna and Gupta¹¹ studied the dynamic stability behavior of piezoelectric layered composite plate utilizing modified first-order shear deformation theory. Bhowal *et al.*¹² studied the dynamic stability of woven fiber laminated composite in hydrothermal environment using first-order shear deformation theory. The nonlinear stability of perforated restrained nanobeams has been analyzed using nonlinear strain gradient elasticity theory, revealing impacts of size effects, perforation, and elastic medium parameters.¹³ The stability of FGM conical shells under combined loads is analyzed using the Pasternak formulation and Galerkin method, highlighting the effects of boundary conditions, material gradients, and elastic formulation.¹⁴ The stability of three-layered truncated conical shells with FG layers under external pressure is analyzed via the Galerkin method, emphasizing the effects of material distribution, FG layer thickness, and geometry.¹⁵ Investigation of the critical dependencies on delamination length and position has been shown by the analysis of the dynamic stability of delaminated composite beams utilizing multi-frequency techniques. FE discretization, and higher-order shear deformation theories,¹⁶ Studies on rotating FG-CNTBC cylindrical shells have shown that free vibration behavior analysis using FSDT and the Rayleigh-Ritz method while considering Coriolis and centrifugal effects, is strongly influenced by CNT content, geometry, and boundary conditions.¹⁷ Similarly, a unified approach for FG-CGPLIC shallow shells demonstrated that GPL weight fraction, layer number, and boundary stiffness significantly affect natural frequencies, with results validated against existing literature.¹⁸ In another investigation, nonlinear forced vibrations of porous FGM sandwich cylindrical shells revealed that porosity distribution, thickness ratio, and external excitations play a crucial role in determining the nonlinear vibration response.¹⁹ Moreover, Zhang *et al.*²⁰ investigated the buckling behavior of rectangular orthotropic thin plates with non-classical boundary restraints, which was analyzed using the finite Fourier integral transform method, which converted governing equations into solvable algebraic forms and produced results consistent with FEM.

A novel FE model based on the discrete-layer approach for laminated beams has been formulated to simulate the bonding and vibration response of laminated beams, mainly focusing on ply damage.^{21,22} The mechanical behavior of basalt and carbon fiber reinforced composite laminate has been investigated, considering FE and an artificial neural network for the beam-to-column joint.²³ Another study introduces a comprehensive approach to predict laminate failure accurately under compressive loads, combining multiscale failure models and structural analysis techniques.^{21,25} The influence of fiber orientation and loading correlation parameters on mesh-square displacement has been analyzed, and results are compared to Kirchhoff and Mindlin's theory.^{26,27} Numerical and experimental analysis demonstrate an intricate relationship between plate orthotropy, boundary conditions, and geometric parameters in composite plates.^{28,29} A finite element analysis (FEA) method has also been developed to predict damage initiation and propagation

A. K. Saha *et al.*

In laminated composite plates under forced vibration and impact loads, and the influence of temperature, magnetic, and electric potentials is revealed by analyzing nonlinear forced vibrations in composite cylindrical shells utilizing Galerkin techniques, Maxwell equations, and modified Donnell shell theory.³² Zhu *et al.*³³ studied the phenomenon of vibration attenuation in rotating thin disks with Acoustic Black Holes (ABH) indentations modeled via Rayleigh-Ritz, Kirchhoff plate theory, and Fourier series. The vibrational behavior of composite shells filled with CNT and graphene nanoplatelets was examined using shell theory, shear deformation theory, Hamilton's principle, and the differential quadrature method, showing that filler distribution and agglomeration strongly influence the dynamics of the shells.³⁴ The transient response of porous viscoelastic nanobeam under dynamic loading and magnetic fields reported that porosity, damping, and magnetic intensity significantly influence oscillation and stability of the shells.³⁵ Furthermore, buckling and vibration of carbon nanotube-reinforced laminated plates were examined with convolution-based methods, emphasizing the roles of nanotube distribution, boundary conditions, and geometry.³⁶ Likewise, Sofaei *et al.*³⁶ analyzed CNT-reinforced composite plates through GDDQ and FEM, revealing a strong dependence of natural frequencies on CNT content, geometry, and boundary conditions. More broadly, meshfree methods have proven effective in static and dynamic analyses, with findings underscoring the role of geometry, boundary conditions, and material distributions in structural performance.³⁸ The transient response of moving composite laminates under mechanical load and high-intensity laser irradiation has also been investigated. Results showed that laser intensity and irradiated surface influence, with higher laser power, do not guarantee greater vibration oscillation or reduction.⁴⁰ A non-destructive method employing impulse excitation techniques provided a means to accurately detect the mechanical parameters of laminated composite plates.⁴¹ In a novel exploration, metastable chaos occurrence has been analyzed in bistable asymmetric laminated composite square shallow shells under foundation excitation. The critical condition is derived based on potential well evolution, highlighting the role of parametric excitation in inducing metastable phenomena.⁴² Porous-core microplates with graphene nanoplatelet patches showed increased stiffness and frequencies with graphene, but reductions due to porosity.⁴³ Mahmood *et al.*⁴⁴ investigate the nano/micro-scale plates, highlighting the influence of nonlocality, geometry, porosity, and reinforcement distribution on vibration behavior, addressing the shortcomings of classical models. In the case of orthotropic thin plates with rotational restraints, the use of a refined Fourier integral transform formulation provided accurate benchmark solutions and provided a detailed understanding of the influence of boundary conditions, fixity, and load ratios.⁴⁵ Further, data-driven approaches have refined vibration modeling, where *iso-geometric analysis* with machine learning models enabled efficient simulation of *cracked laminated plates*, corrugated and flat annular plates, and Miura-folded

Dynamic Stability Behavior Prediction

composite shells, providing valuable insights on the effects of cracks, layup, holes, and boundary conditions while emphasizing the benefits of helical and orthogonal inspired designs.^{46, 48} Similarly, auxetic piezoelectric harvesters have been shown to outperform conventional systems due to their negative Poisson's ratio, offering both efficiency and scalability.⁴⁹ In the field of additive manufacturing, reviews of aluminum alloys, AMCs, and polymer matrix composites emphasize the impact of process parameters, reinforcements, and techniques such as FDM and SLA, though issues in fatigue, defects, and optimization persist.⁵⁰ Further, Armand *et al.*⁵² studies on epoxy nanocomposite reinforced with Ni_3O_4 nanoparticles report significant gains in tensile and adhesive strength at optimal loading, while predictive models further enhance performance evaluation. Studies on shear buckling of functionally graded skew plates demonstrated that both reinforcement and skew angle play a decisive role in governing the critical buckling response.⁵³ Thermoelastic coupling in viscoelastic media with cavities under magnetic fields was modeled using the Moser-Gibson-Thompson framework, which reveals the effects of Hall currents, viscosity, and thermal fluctuations.⁵⁴

The instability zone predicts flutter and resonance in aircraft wings and fuselage panels, helping in preventing structural failure.⁵⁵ Rotor shafts in turbines, helicopters and jet engines undergo parametric resonance; recognizing eigenfrequencies aids in designing safer rotating machinery and preventing catastrophic failure.⁵⁶ Gear system and rotating discs undergo periodic excitations; knowing the instability zone helps in preventing sudden failure.⁵⁷ These studies collectively contribute to a deeper understanding of the complex behavior exhibited by laminated composite structures under various loading and excitation conditions, offering insights crucial for their design and application. The current investigation has developed a mathematical model to analyze the excitation frequency response for the intact and damaged (cracked) structures. The discretization approach using finite elements creates a higher-order kinematic model to evaluate the parametric instability, considering a nine-noded isoparametric element with nine degrees of freedom per node. The differential equations of motion of the system are transformed into a set of ordinary differential equations and solved as an ordinary eigenvalue solution. The reliability of the numerical model is validated by correlating the behavior of a planar sheet structure subjected to dynamic instability. Subsequently, the framework is adapted to various geometrical shapes to assess its feasibility and flexibility in analyzing dynamic instability response. Further, the verified numerical model is utilized to evaluate the various design parameters influencing the dynamic instability of the laminated structures.

2. Mathematical Formulation

The curved structure possessing span length of ' l_1 ', width ' l_2 ' and depth ' h ' is assumed to be positioned in the directions of principal material axes, i.e. α , β ,

A. K. Saha et al.

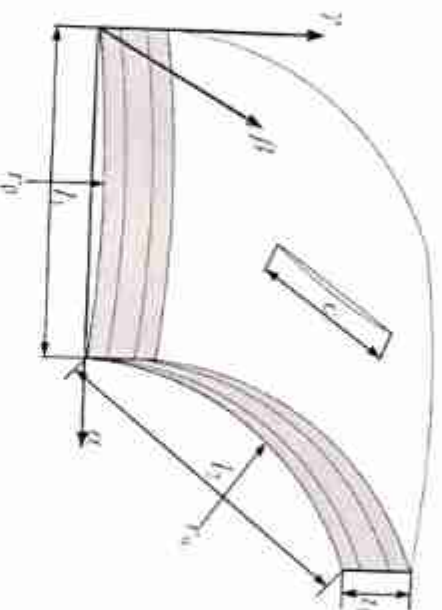


Fig. 1. Layers of the multi-layered curved structure.

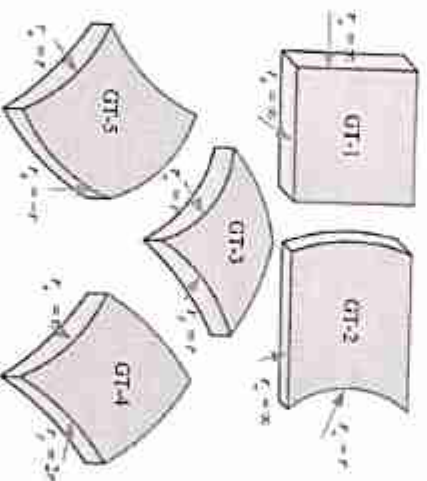


Fig. 2. Diverse configurations of the structure.

and z -axes, respectively, as shown in Fig. 1. The curved panel is assumed to be the combination of n numbers of layers having curvature parameters stated as, ' r_{α} ' and ' r_{β} ' along the principal axes (β - and α -axis). The various geometrical structure forms can be obtained by altering the radius of curvature along the α and β axes (refer to Fig. 2). In order to have clarity about the geometries, a detailed abbreviation of various forms is delineated in Table 1.

Table 1. Details of various geometries.

| Geometrical shapes | Presentation in analysis |
|--------------------|--------------------------|
| GT-1 | Plate |
| GT-2 | Cylindrical |
| GT-3 | Spherical |
| GT-4 | Hyperboloid |
| GT-5 | Elliptical |

The displacement polynomial used for kinematics employed in this study is $u_{\alpha\beta\gamma}^{(0)}$

$$\begin{Bmatrix} U_{\alpha\alpha} \\ V_{\beta\beta} \\ W_{\gamma\gamma} \end{Bmatrix} = \begin{Bmatrix} u_{\alpha\alpha}^{(0)} \\ v_{\beta\beta}^{(0)} \\ w_{\gamma\gamma}^{(0)} \end{Bmatrix} + \begin{Bmatrix} \theta_{\alpha\alpha}^{(1)} \\ \theta_{\beta\beta}^{(1)} \\ D \end{Bmatrix} \gamma + \begin{Bmatrix} \Lambda_{\alpha\alpha}^{(2)} \\ \Lambda_{\beta\beta}^{(2)} \\ 0 \end{Bmatrix} \gamma^2 + \begin{Bmatrix} \psi_{\alpha\alpha}^{(3)} \\ \psi_{\beta\beta}^{(3)} \\ 0 \end{Bmatrix} \gamma^3. \tag{1}$$

Or,

$$\begin{aligned} u_{\alpha\alpha}^{(0)} &= u_0(\alpha, \beta, t), & v_{\beta\beta}^{(0)} &= \theta_0(\alpha, \beta, t), & w_{\gamma\gamma}^{(0)} &= u_0(\gamma_{\alpha\alpha}, \gamma_{\beta\beta}, t), & \theta_{\alpha\alpha}^{(1)} &= (\theta_{0\alpha\alpha}/\partial\gamma), \\ \theta_{\beta\beta}^{(1)} &= (\theta_{0\beta\beta}/\partial\gamma), & \Lambda_{\alpha\alpha}^{(2)} &= 1/2(\partial^2 \Lambda_{\alpha\alpha}/\partial\gamma^2), & \Lambda_{\beta\beta}^{(2)} &= 1/2(\partial^2 \Lambda_{\beta\beta}/\partial\gamma^2), \\ \psi_{\alpha\alpha}^{(3)} &= 1/6(\partial^3 \psi_{\alpha\alpha}/\partial\gamma^3), & \psi_{\beta\beta}^{(3)} &= 1/6(\partial^3 \psi_{\beta\beta}/\partial\gamma^3). \end{aligned}$$

The displacement at a given point along the principal directions (α, β , and γ) is represented by $U_{\alpha\alpha}$, $V_{\beta\beta}$, and $W_{\gamma\gamma}$, respectively. The rotational displacements of the normal about the panel mid-plane along β - and α -axes are represented by $\theta_{\alpha\alpha}$ and $\theta_{\beta\beta}$, respectively. In addition, the terms $\Lambda_{\alpha\alpha}$, $\Lambda_{\beta\beta}$, $\Psi_{\alpha\alpha}$ and $\Psi_{\beta\beta}$ are used to maintain the necessary continuity of shear strain and stresses.

Moreover, to establish the constitutive behavior of a layered component for any n th lamina oriented at any angle (ϕ) is expressed as:

$$\begin{Bmatrix} S_{\alpha\alpha} \\ S_{\beta\beta} \\ S_{\gamma\gamma} \\ \xi_{\alpha\beta} \\ \xi_{\alpha\gamma} \\ \xi_{\beta\gamma} \end{Bmatrix} = \begin{pmatrix} T_{11} & T_{12} & T_{13} & 0 & 0 & 0 \\ T_{21} & T_{22} & T_{23} & 0 & 0 & 0 \\ T_{31} & T_{32} & T_{33} & 0 & 0 & 0 \\ 0 & 0 & 0 & T_{00} & 0 & 0 \\ 0 & 0 & 0 & 0 & T_{55} & 0 \\ 0 & 0 & 0 & 0 & 0 & T_{44} \end{pmatrix} \begin{Bmatrix} \zeta_{\alpha\alpha} \\ \zeta_{\beta\beta} \\ \zeta_{\gamma\gamma} \\ \zeta_{\alpha\beta} \\ \zeta_{\alpha\gamma} \\ \zeta_{\beta\gamma} \end{Bmatrix} \tag{2}$$

$$\text{or, } \{S\} = [\bar{T}]\{\zeta\}, \tag{3}$$

where $[\bar{T}]$ and $\{S\}$ are matrices representing reduced transformed stiffness and the stress matrices, respectively.

A. K. Sabu et al.

The strain-displacement relations are used as²⁸

$$\{\zeta\} = \begin{pmatrix} \zeta_{\alpha\alpha} \\ \zeta_{\beta\beta} \\ \zeta_{\gamma\gamma} \\ \zeta_{\alpha\beta} \\ \zeta_{\alpha\gamma} \\ \zeta_{\beta\gamma} \end{pmatrix} = \begin{bmatrix} \frac{\partial U_{\alpha\alpha}}{\partial x} + \frac{W_{\gamma\gamma}}{R_\alpha} \\ \frac{\partial W_{\beta\beta}}{\partial \beta} + \frac{W_{\gamma\gamma}}{R_\beta} \\ \frac{\partial W_{\gamma\gamma}}{\partial \gamma} \\ \frac{\partial U_{\alpha\alpha}}{\partial \beta} + \frac{\partial W_{\beta\beta}}{\partial x} + \frac{2W_{\gamma\gamma}}{R_{\alpha\beta}} \\ \frac{\partial U_{\alpha\alpha}}{\partial \gamma} + \frac{\partial W_{\gamma\gamma}}{\partial \alpha} - \frac{U_{\alpha\beta}}{R_\alpha} \\ \frac{\partial W_{\alpha\alpha}}{\partial \gamma} + \frac{\partial W_{\gamma\gamma}}{\partial \beta} - \frac{V_{\beta\beta}}{R_\beta} \end{bmatrix} \quad (4)$$

Now using Eq. (1) in Eq. (3), it is further modified as

$$\{\bar{\zeta}\} = \begin{pmatrix} \zeta_{\alpha\alpha} \\ \zeta_{\beta\beta} \\ \zeta_{\gamma\gamma} \\ \zeta_{\alpha\beta} \\ \zeta_{\alpha\gamma} \\ \zeta_{\beta\gamma} \end{pmatrix} + \zeta \begin{pmatrix} k_{\alpha\alpha}^1 \\ k_{\beta\beta}^1 \\ 0 \\ k_{\alpha\beta}^1 \\ k_{\alpha\gamma}^1 \\ k_{\beta\gamma}^1 \end{pmatrix} + \zeta^2 \begin{pmatrix} k_{\alpha\alpha}^2 \\ k_{\beta\beta}^2 \\ 0 \\ k_{\alpha\beta}^2 \\ k_{\alpha\gamma}^2 \\ k_{\beta\gamma}^2 \end{pmatrix} + \zeta^3 \begin{pmatrix} k_{\alpha\alpha}^3 \\ k_{\beta\beta}^3 \\ 0 \\ k_{\alpha\beta}^3 \\ k_{\alpha\gamma}^3 \\ k_{\beta\gamma}^3 \end{pmatrix} \quad (5)$$

Further, Eq. (4) can be written as

$$\text{or, } \{\zeta\} = [X_d]\{\bar{\zeta}\}, \quad (6)$$

where $[X_d]$ is thickness coordinate matrix.

2.1. Discretization and crack formation

For numerical analysis, the laminate structure consists of a crack through-thickness in the γ -direction. The global α, β -direction specifies the necessary cut dimension. The center of the specimen is considered the source for the meshing of the structure. Nine-noded (Fig. 3(a)) rectangular isoparametric elements with nine degrees of freedom for each node has been used to obtain the meshing of the structure. The meshing of the first quadrant is depicted in Fig. 3(b). The mirror image approach in MATLAB is used to obtain the meshing of the second quadrant. Lastly, by mirroring the discretization around the α -axis, the meshing of the entire structure (Fig. 3(c)) is achieved.

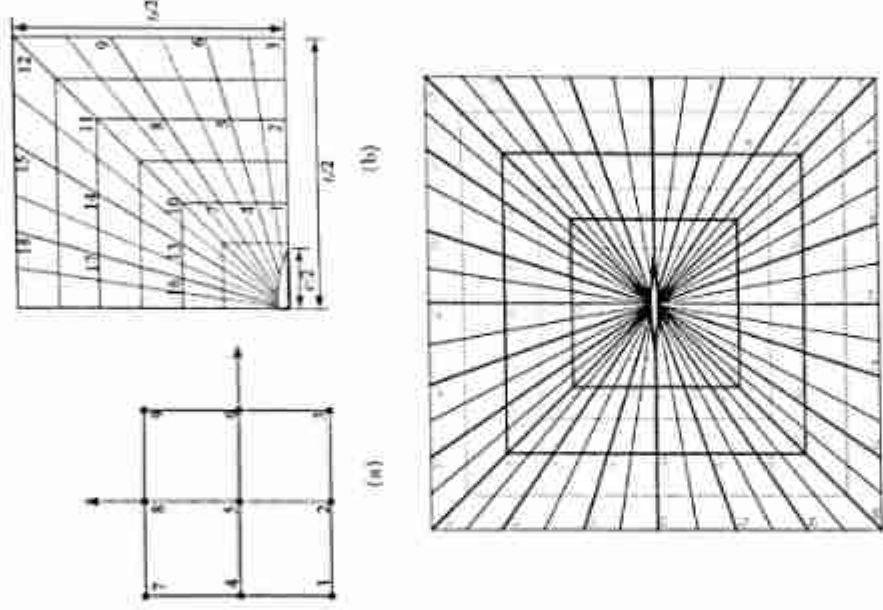


Fig. 3. (a) Nine-noded element (b) Meshed first quadrant (c) Meshed entire structure.

The FE formulation of the curved panel component is derived by incorporating a nine-noded isoparametric element, and each node has nine degrees of freedom (DOFs).

$$\{q\} = \sum_i N_i \{q_i\} \quad x = \sum_i N_i x_i \quad y = \sum_i N_i y_i \quad (7)$$

where $\{q\}$ and x_i and y_i are the multi-dimensional state variable and the nodal coordinate values of the corresponding i th node, respectively. Also, the term N_i is representing the interpolation function.

Now, to compute the total deformation of the panel component under the dynamic loading, different energy expressions are obtained by evaluating the kinetic

A. K. Sahin et al.

energy expression, including the density and velocity values as

$$K_c = \frac{1}{2} \int_V \rho (\dot{U}_\alpha^2 + \dot{V}_\beta^2 + \dot{W}_\gamma^2) dV = \frac{1}{2} \int_A \{r\}^T [N]^T [I] [N] \{r\} dA. \quad (8)$$

The expression contains $[N]$ is representing the thickness coordinate matrix for the consistent mass matrix and the corresponding inertia matrix. i.e. $I = \sum_{k=1}^n \int_{-h}^h \rho^k \{\phi\}^T \{\phi\} dz$, n is the total number of laminate in the structure.

The strain energy of the laminated composite structure can be expressed as

$$S_c = \frac{1}{2} \int_V \{s\}^T [S] dV + \frac{1}{2} \int_V \{\gamma\}^T \{\tau\} dV. \quad (9)$$

The above equation can also be represented as

$$S = \frac{1}{2} \int_A \{q\}^T [D^s] [D^s] \{q\} dA + \frac{1}{2} \int_A \{q\}^T [D^s] [D^s] [B^s] \{q\} dA. \quad (10)$$

The potential energy due to applied non-uniform in-plane loading can be written as

$$P_c = \frac{1}{2} \int_V \left\{ \bar{L}_{\alpha\alpha} \left(\frac{\partial U_{\gamma\gamma}}{\partial \alpha} \right)^2 + L_{\alpha\alpha} \left(\frac{\partial U_{\gamma\gamma} \partial U_{\alpha\alpha}}{\partial \alpha \partial \beta} \right) + \bar{L}_{\beta\beta} \left(\frac{\partial U_{\alpha\alpha}}{\partial \alpha} \right)^2 \right\} dV, \quad (11)$$

where the terms are expressed in the above equation, i.e. $L_{\alpha\alpha}$, $L_{\beta\beta}$ and $L_{\alpha\beta}$ are the stresses (in-plane) developed within the laminate due to the non-uniform edge loading provided along the in-plane.

Now, Eq. (10) can be rewritten as

$$P_c = \frac{1}{2} \int_V \begin{Bmatrix} W_{\alpha\alpha} \\ W_{\beta\beta} \end{Bmatrix}^T \begin{Bmatrix} L_{\alpha\alpha} & L_{\alpha\beta} \\ L_{\alpha\beta} & L_{\beta\beta} \end{Bmatrix} \begin{Bmatrix} W_{\alpha\alpha} \\ W_{\beta\beta} \end{Bmatrix} dV = \frac{1}{2} \int_A \{q\}^T [B^s]^T [S^s] [B^s] \{q\} dA, \quad (12)$$

where $[B^s]$ and $[S^s]$ are the differential operator and the in-plane stress matrix.

The final form of the desired governing equations of the panel to count the parametric stability can be obtained using the following expression:

$$\frac{d}{dt} \left(\frac{\partial K_c}{\partial \{r\}} \right) + \frac{\partial S_c}{\partial \{r\}} - \frac{\partial P_c}{\partial \{r\}} = 0, \quad (13)$$

where r is the overall state variable, S_c , K_c and P_c denote the gross strain energy, gross kinetic energy and gross potential energy of the laminated composite plate, respectively, due to the applied in-plane external load.

By inserting the corresponding terms of energy into Eq. (13) and differentiating, the resulting expression is derived as

$$[I] \{\dot{r}\} + \{[K] - [K_{nl}]\{r\}\} = 0, \quad (14)$$

where

$$[U] = \int_A [N]^T [U] [N] dA, \quad [K] = \int_A ([U]^T [P^s] [U^s] + [U]^T [P^d] [U^d]) dA$$

and

$$[P^s] = \sum_{i=1}^n \int_{\Omega_i} [U^s]^T [Q_i^s] [U^s] dx, \quad [P^d] = \sum_{i=1}^{n-1} \int_{\Omega_i} [U^d]^T [Q_i^d] [U^d] dx$$

$$[K_g] = \int_A [U]^T [S^g] [U] dA \tag{15}$$

Here, $[U]$ is the overall generalized mass matrix, $[K]$ is the global system stiffness matrix, $[K_g]$ is the geometric stiffness matrix.

Equation (14) can now be reformulated using the in-plane external load source expression⁶⁰:

$$[U]\{\ddot{r}\} + ([K] - [P_s + P_d \cos \Delta_e t] [K_g])\{r\} = 0 \tag{16}$$

where P_s and P_d are the parts of total externally applied force $\{P\}$. Similarly, the term Δ_e represents the non-dimensional form of the frequency parameter due to external excitation.

Further, to calculate the critical load due to buckling while the structure/structural components are under the influence of any externally applied in-plane loads,

$$P_s = \mu_s L_{cr} \quad \text{and} \quad P_d = \mu_d L_{cr} \tag{17}$$

where L_{cr} underscores the load at the buckling threshold of the structure. In addition, a few more factors are shown in the above equation representing the static (μ_s) and dynamic (μ_d) load factors.

Further, the final form of governing equation is obtained by putting the values of forces (observed in Eq. (14) in Eq. (13)) and modified as⁶⁰:

$$[U]\{\ddot{r}\} + ([K] - \mu_s L_{cr} [K_g] - \mu_d L_{cr} \cos \Delta_e t [K_g])\{r\} = 0 \tag{18}$$

Equation (18) is termed a Mathieu-type differential equation, and the solution obtained from the same will provide the details about the dynamic instability of any structural component.

Now, the necessary solutions are being done by using the Fourier series with the help of two simultaneous periodic equations (19) and (20). Additionally, two-time periodic interval as T and $2T$; $T = \frac{2\pi}{\Delta_e}$.

$$\{r_i\} = \sum_{i=1}^{\infty} \left[\alpha_i \sin \frac{(2i-1)\Delta_e t}{2} + \beta_i \cos \frac{(2i-1)\Delta_e t}{2} \right] \tag{19}$$

A. K. Saha *et al.*

$$[r_1] = \frac{1}{2} n_0 + \sum_{i=1}^{\infty} \left[\alpha_i \sin \frac{(2i)\Delta_c t}{2} + \beta_i \cos \frac{(2i)\Delta_c t}{2} \right], \quad (20)$$

where α_i and β_i represent arbitrary constants.

The primary estimate of the instability zone is provided by the following expression:

$$\left| \{[K] - \mu_s L_{cr}[K_0] \pm 0.5\mu_d L_{cr}[K_0]\} - \frac{\Delta_c^2}{4} [H] \right| = 0. \quad (21)$$

The greatest and least Δ_c are determined by individually altering between the signs in Eq. (21).

The secondary instability region can potentially be derived by computing the eigenvalues in the following manner:

$$\begin{aligned} & \{[K] - \mu_s L_{cr}[K_0]\} - \Delta_c^2 [M] = 0, \\ & \left| \left[\begin{array}{c} \{[K] - \mu_s L_{cr}[K_0]\} - \mu_d L_{cr}[K_0] \\ -0.5\mu_d L_{cr}[K_0] \end{array} \right] \{[K] - \mu_s L_{cr}[K_0]\} - \left[\begin{array}{c} [0]_{d \times d} \\ [0]_{d \times d} \end{array} \right] [H] \right| = 0. \end{aligned} \quad (22)$$

For the computational analysis, different end boundaries are implemented, and the details can be seen in Table 2.

Table 2. Details of boundary condition.

| End condition | Symbolic | Particulars |
|---|----------|--|
| SSSS (Simple support end boundary condition) | C0 | $w_0 = \theta_{0,0} = \Delta_{s,0} = \Psi_{0,0} = \Psi_{0,0} = w_0 = \theta_{0,0} = 0$ at $\alpha = 0$ and l_1 $= \Delta_{s,l} = \Psi_{l,0} = w_0 = \theta_{0,l} = 0$ at $\beta = 0$ and l_2 |
| CCCC (All Clamped) | C1 | $w_0 = \theta_{0,0} = \Delta_{s,0} = \Psi_{0,0} = w_0 = \theta_{0,0} = 0$ at $\alpha = 0$ $= \Delta_{s,l} = \Psi_{l,0} = w_0 = \theta_{0,l} = 0$ |
| SCSC (Simple support clamped, simple support clamped) | C2 | $w_0 = \theta_{0,0} = \Delta_{s,0} = \Psi_{0,0} = w_0 = \theta_{0,0} = 0$ at $\alpha = 0$ and l_1 l_2 |
| CFF (Clamped, fixed, fixed) | C3 | $w_0 = \theta_{0,0} = \Delta_{s,0} = \Psi_{0,0} = w_0 = \theta_{0,0} = 0$ at $\alpha = 0$ and l_1 $= \Delta_{s,l} = \Psi_{l,0} = w_0 = \theta_{0,l} = 0$ |
| SFSF (Simple support, fixed, fixed simple support) | C4 | $w_0 = \theta_{0,0} = \Delta_{s,0} = \Psi_{0,0} = w_0 = \theta_{0,0} = 0$ at $\alpha = 0$ and l_1 l_2 $w_0 = \theta_{0,0} = \Delta_{s,0} = \Psi_{0,0} = w_0 = \theta_{0,0} = 0$ at $\beta = 0$ and l_2 $\theta_{s,0} = \Delta_{s,0} = \Psi_{s,0} = w_0 = \theta_{s,0} = 0$ at $\beta = 0$ and l_2 |
| CFCF (Clamped-fixed Clamped fixed) | C5 | $w_0 = \theta_{0,0} = \Delta_{s,0} = \Psi_{0,0} = w_0 = \theta_{0,0} = 0$ at $\alpha = 0$ and l_1 l_2 |

3. Results and Discussions

The convergence study is conducted initially to verify the consistency of the developed mathematical model and subsequent computational code. The frequency response under excitation has been analyzed for different static load factors (μ_s) across different mesh variations in density, ranging from 1×1 to 7×7 . Initially, the numerical model has been developed with the geometrical properties $l_1 = l_2 = 1$ m, thickness ratio (l_1/t_1) = 200, curvature ratio (r/l_1) = 40, $\mu_s = 0.4$, layup sequence $[0^\circ/90^\circ]_4$ and each layer of the layup is assigned with the material properties $E_{11}/E_{22} = 40$, $G_{12}/E_{22} = 0.6$, $G_{13}/E_{22} = 0.6$, $G_{23}/E_{22} = 0.5$, $\nu_{12} = 0.25$. The crack introduced in each of the structures under analysis has the following dimensions: $r_a = 0.03$ m and $r_b = 0.001$ m. The non-dimensional excitation frequency response is evaluated under simple support end boundary conditions by varying the mesh densities, and the obtained results are presented in Fig. 4. The convergence result indicates that the developed mathematical model predicts the excitation frequency response with minimal deviation compared to the previous iteration response. The responses are evaluated by varying the mesh densities; beyond the mesh size of elements 3×3 , they demonstrate consistent behavior. Hence, a 4×4 element mesh size is finalized to assess the dynamic excitation frequency response. Further, to explore excitation frequency behavior of shell-type curved structures without compromising accuracy or computational efficiency, a mesh size of 4×4 is consistently employed during the entire study.

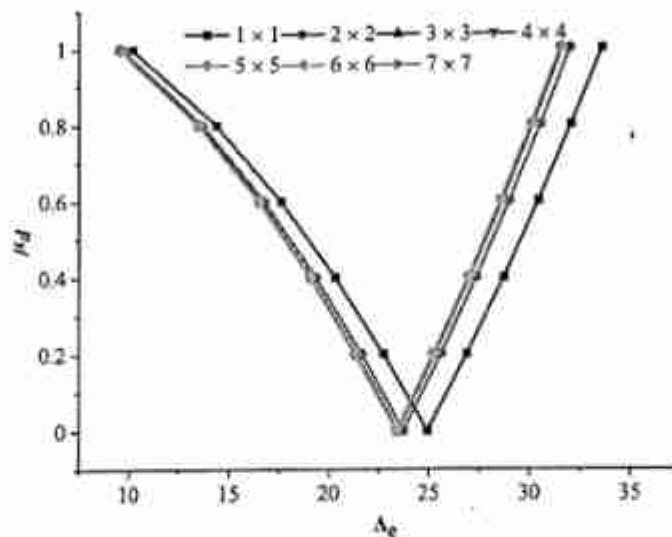


Fig. 4. Convergence response of the multi-layered curved shell framework.

A. K. Sabu et al.

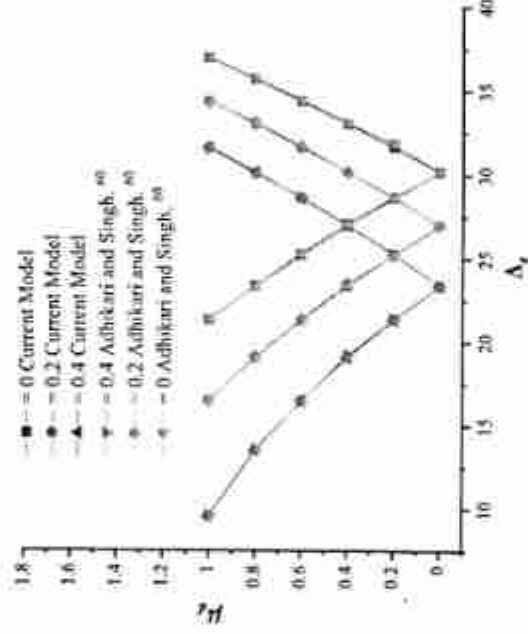


Fig. 5. Comparative analysis of responses under dynamic instability conditions of planar sheet structure using current developed model.

Further, a comparison study has been conducted to verify the numerical model's efficiency in evaluating the response to non-dimensional excitation frequency. To check the correctness of the developed numerical model, the geometrical parameters are as follows: $l_1 = l_2 = 1$ m, $l_1/l_1 = 200$, layup sequence $[0^\circ/90^\circ]_4$. The characteristics of material for each layup are assigned as $E_{11}/E_{22} = 40$, $G_{12}/E_{22} = 0.6$, $G_{23}/E_{22} = 0.5$, $\nu_{12} = 0.25$ from Ref. [60]. The responses of the excitation frequency for laminated composite structures have been assessed under different static and dynamic load factors, and the obtained results are compared with those of Adhikari and Singh [60] in Fig. 5. The comparison of the numerical excitation frequency response demonstrates a negligible deviation in the non-dimensional form of frequency parameter due to external excitation response. The developed numerical model exhibits 10.31% of deviation from the reference result. Hence, it confirms that the accuracy of the developed mathematical model is robust enough to predict the responses of the non-dimensional excitation frequency.

3.1. Additional illustrations

The verified numerical model is extended to analyze the excitation frequency (Δt) response of diverse geometric parameters pertaining to the curved shell panel. This rigorous analysis uncovered a multitude of implications stemming from variations

Dynamic Stability Behavior Prediction

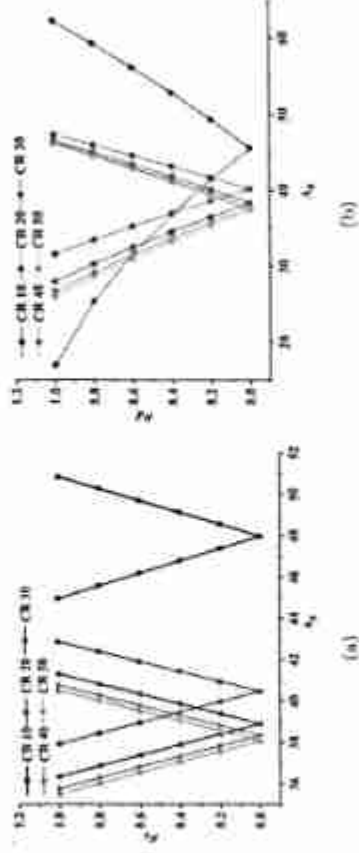


Fig. 8. Influence of CR on DIR of cylindrical shell panel under $\mu_s = 0.1$. (a) Intact, (b) Crack.

in static and dynamic load factors. It is noteworthy that the geometric and elastic properties remained invariant throughout the study, with parameters set as follows:⁶⁰ $l_1 = l_2 = 1$ m, $I_1/I_2 = 200$, layup sequence $[0^\circ/90^\circ]_4$, $E_{11}/E_{22} = 40$, $G_{12}/E_{22} = 0.6$, $G_{23}/E_{22} = 0.6$, $G_{31}/E_{22} = 0.5$, $\nu_{12} = 0.25$, and $\rho = 1$ kg/m³. In this study, the crack dimensions are taken as $r_a = 0.003$ m and $r_b = 0.001$ m. The crack is positioned at the center of the shell panel, and the effect of its orientation on the excitation frequency response is not considered. The effect of various design parameters on the excitation frequency response is analyzed under a simple support end boundary condition (C0).

3.1.1. Effect of curvature ratio (CR) on cylindrical shell

The influence of CR on the Dynamic Instability Region (DIR) of a cylindrical shell panel under a static load factor $\mu_s = 0.1$ is studied for both intact and crack cases, and the obtained results are presented in Fig. 6. In the intact case (Fig. 6(a)), the DIR exhibits a symmetric “V”-shaped pattern for all CR, centered around $\Delta_s \approx 40$, indicating consistent modal behavior and structural stiffness across the panel. However, in the crack case (Fig. 6(b)), noticeable asymmetry emerges, especially at lower CRs such as CR 10 and CR 20. The existence of a crack in the shell panel reduces its local stiffness, resulting in disrupting the symmetry and widening of DIR, with the instability shifting away from the expected central region. Interestingly, panels with higher CRs (CR 40 and CR 50) show a tendency to restore symmetry and narrow DIR, highlighting the stabilizing influence of increased geometric stiffness. This indicates that the presence of a crack reduces the dynamic stability of the shell panel. However, an increase in the curvature ratio (CR) enhances structural integrity by weakening the effect of the crack and thereby improving the panel’s resistance against parametric excitation.

A. K. Saboo et al.

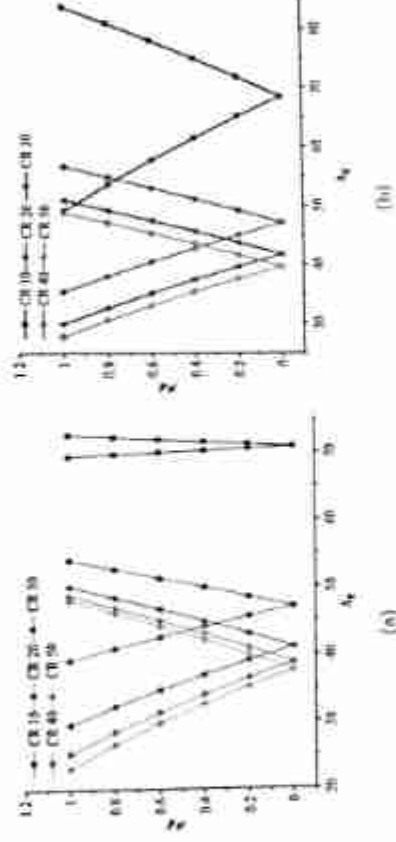


Fig. 7. Influence of CR on DIR of spherical shell panel under $\mu_s = 0.1$, (a) Intact, (b) Crack.

3.1.2. Effect of CR on a spherical shell

The effect of CR on the DIR of spherical shell panel subjected to a static load factor $\mu_s = 0.1$ is presented in Fig. 7. The results are shown for both intact and cracked configurations to elucidate the influence of geometric curvature and damage on the dynamic stability characteristics of spherical shells. In case of intact condition (Fig. 7(a)), the DIR exhibits a symmetric "V"-shaped profile centered around $\Delta_s \approx 45$, with narrower and deeper stable regions observed at higher CRs due to increased geometric stiffness. However, the presence of a crack in the shell panel (Fig. 7(b)) reduces structural stiffness, resulting in a wider and asymmetric DIR compared to the intact case. Furthermore, a lower CR tends to flatten the shell panel, allowing the crack to dominate the stiffness response and produce a wider DIR, as observed for CR 10. In contrast, higher CRs (CR 40 and 50) demonstrate improved damage tolerance, with DIRs closely resembling the intact case.

3.1.3. Effect of boundary condition

The influence of different boundary conditions (C-0 to C-5) on the DIR of the shell panel under $\delta = 0.1$, for both intact and crack cases, is illustrated in Fig. 8. Boundary condition variations significantly alter the DIR characteristics due to their direct impact on constraint stiffness and modal restraint. The curved shell panel of the intact case (Fig. 8(a)) with boundary constraints C-1, C-2, and C-5 shows a narrower and deeper "V"-shaped DIRs centered at higher Δ_s values, reflecting increased structural stiffness and delayed onset of resonance. Conversely, the boundary conditions, C-0, C-3, and C-4 are the flexible boundary conditions that allow the structure lowers bending-membrane coupling and alters mode shapes, leading to weaker energy transfer from excitation to instability growth. Similarly,

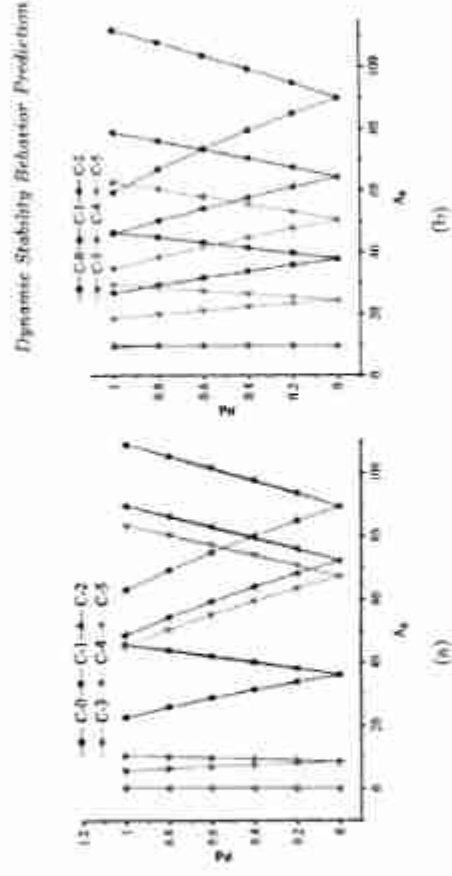


Fig. 8. Impact of boundary conditions on DIR of cylindrical shell panel under $\mu_s = 0.1$, (a) Intact, (b) Crack.

the influence of various boundary conditions on the crack case (Fig. 8(b)) follows the same trend.

3.1.4. Effect of geometry

This section presents the effect of geometric variation (GT-1 to GT-5) on the DIR of constant curvature shell panels subjected to a static load factor $\mu_s = 0.1$. In the intact condition (Fig. 9(a)), panels with optimized geometric proportions (GT-3, GT-4, GT-5), exhibit narrow and symmetric DIRs, reflecting stable modal interaction and enhanced in-plane stiffness. In contrast, GT-1 and G-3 display a wider DIR with an early onset of instability, indicating that unfavorable geometric configurations reduce dynamic resistance and promote modal coupling. However, in a crack condition (Fig. 9(b)), the overall DIR shape remains symmetric across all geometries, suggesting that certain geometrical configurations inherently resist the destabilizing damage effect and stabilize the shell structure. The crack creates a dominant, localized reduction in stiffness that overwhelms geometry differences; all geometries behave similarly once cracked. Intact panels keep their global stiffness dictated by geometry, so their responses scatter.

3.1.5. Effect of thickness ratio

This section illustrates the influence of thickness ratios ($t_1/t_2 = 20$ to 300) on the non-dimensional excitation frequency responses of cylindrical shell panels, considering $\mu_s = 0.1$. In the case of intact (Fig. 10(a)), the excitation frequency response increases with an increase in the thickness ratio. Thinner shells (higher t_1/t_2) exhibit a narrower DIRs and a delayed onset of instability, attributed to their higher flexibility and lower bending stiffness. Whereas, thicker shells ($t_1/t_2 = 20, 60$) show

A. K. Sahni et al.

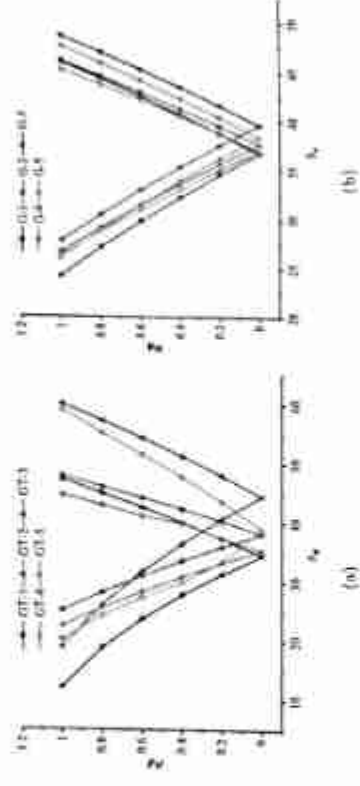


Fig. 9. Influence of geometry on DIR of laminated panel under $\mu_s = 0.1$. (a) Intact, (b) Crack.

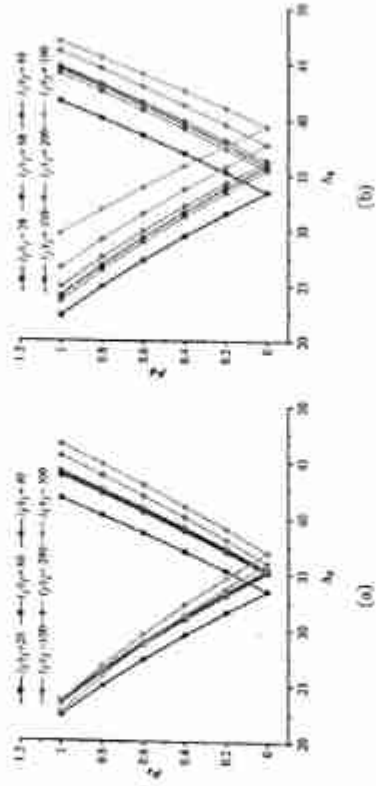


Fig. 10. Influence of thickness ratio on DIR of cylindrical laminated shell panel under $\mu_s = 0.1$. (a) Intact, (b) Crack.

wider DIRs and earlier instability, indicating a stiffer structure more prone to dynamic response due to stronger mode coupling. Correspondingly, in the crack case (Fig. 10(b)), the DIR pattern remains similar; the existence of the crack across thickness introduces slight widening and asymmetry pattern for all thickness ratios. At lower thickness ratios, the shell stiffness increases, which might reduce the crack effect on the dynamic excitation frequency.

3.1.6. Effect of static load factor

The influence of static load factors (μ_s) on the non-dimensional excitation frequency responses of a constant curvature shell structure is analyzed for intact and crack

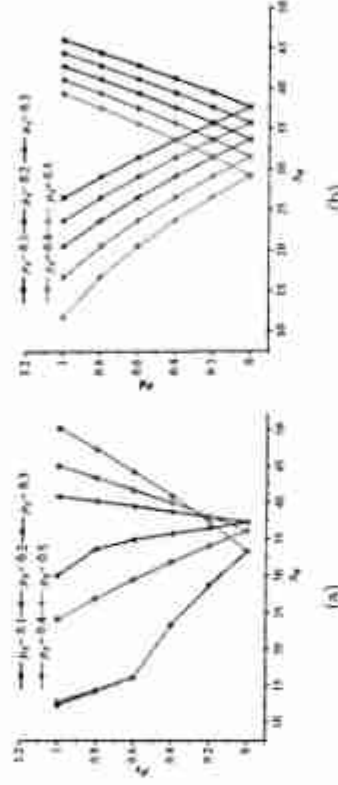


Fig. 11. Effect of static load factor on DIR of cylindrical laminated shell panel under $\mu_s = 0.1$, (a) Intact, (b) Crack.

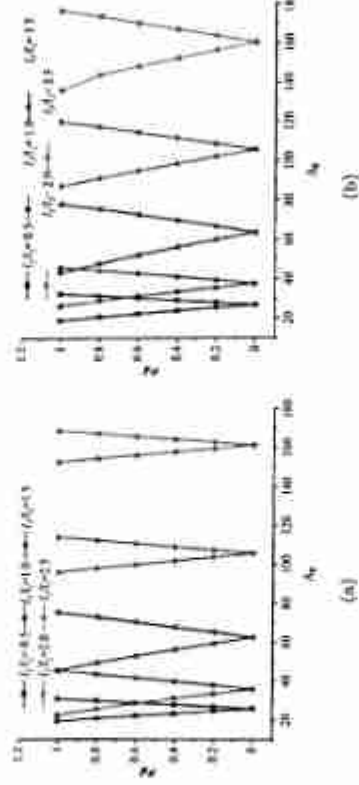


Fig. 12. Influence of aspect ratio on DIR of cylindrical laminated shell panel under $\mu_s = 0.1$, (a) Intact, (b) Crack.

cases. The obtained excitation frequency response is presented in Figs. 11(a) and 11(b). In the case of intact (Fig. 11(a)), increasing μ_s results in significant broadening of the DIR, which indicates the reduced structural stiffness. The higher static loading pre-stresses the shell, lowering its effective stiffness, which results in the earlier onset of parametric resonance. Similarly, in the crack case (Fig. 11(b)), DIRs indicate that the widening trend persists, but the curves shift more uniformly. The presence of a crack in the panel reduces local stiffness, compounding the destabilizing effect of static loading.

3.1.7. Effect of aspect ratio

The influence of aspect ratios (l_1/l_2) on the DIR considering constant curvature of cylindrical shell panel under $\mu_s = 0.1$ is presented in Fig. 12. In the intact

A. K. Sahu et al.

case (Fig. 12(a)), increasing aspect ratio leads to a rightward shift in Δ_c and broader spacing of the DIR, indicating that longer panels (i.e. higher l_1/l_2) are dynamically more stable, with delayed onset of parametric instability. Whereas in shorter panels (i.e. $l_1/l_2 = 0.5, 1.0$) show narrower and deeper DIRs due to higher curvature-induced stiffness and lower critical excitation thresholds. Likewise, in the crack case (Fig. 12(b)), a similar trend is observed, but with increased DIR asymmetry at lower aspect ratios. In contrast, shells with $l_1/l_2 \geq 2.0$ exhibit wider spacing between the instability band and maintain symmetry, suggesting that higher aspect ratios reduce sensitivity to damage by dispersing its influence.

4. Conclusion

This study developed a higher-order finite element model to investigate the dynamic instability behavior of laminated curved composite structures with and without cracks under in-plane loads. The model, validated with 10.31% deviation from reference results, highlighted that curvature ratio, geometry, boundary condition, thickness ratio, static load factor, and aspect ratio significantly affect stability. In accordance with the study carried out, the following observations were made:

- The developed higher-order FE model predicts dynamic instability of laminated curved composites accurately, with $\sim 10.31\%$ deviation from reference data.
- Higher CR improves stiffness and narrows instability regions, while lower CR increases instability in cracked structures.
- Clamped edges enhance stability, whereas flexible supports reduce it.
- Spherical and Elliptical shells show better stability than plate-type geometries.
- Thinner shells delay instability onset, while thicker shells trigger it earlier.
- Static load factor reduces effective stiffness and broadens instability zones; cracks amplify this effect.
- Higher aspect ratios improve susceptibility to damage and shift instability to higher frequencies.

This study is limited to single through-thickness cracks in the absence of material damping, and neglect of environmental factors, i.e. influence of temperature and humidity. Furthermore, only numerical simulations were considered, without experimental validation. Future work could incorporate the crack orientation and subsequent propagation, nonlinear material effects, and thermo-hygro-mechanical coupling to enable machine-learning-based predictive accuracy.

This work can be directly applied in the design of aerospace fuselages, wings, and satellite shells, submarine pressure hulls and marine vessels, and defense structures such as missile casings and ramjets, where stability under dynamic loads is critical. It also supports civil applications like composite bridges, tanks, and curved roofs, and can enhance structural health monitoring (SHM) systems for early crack

detection. Further, the model can be embedded into finite element software to assist engineers in reliable and efficient composite design.

ORCID

Ashish Kumar Sahu © <https://orcid.org/0009-0006-8195-806X>
 Ankit Gangwar © <https://orcid.org/0009-0002-0043-2611>
 Naveen Kumar Akkasali © <https://orcid.org/0009-0008-0014-8300>
 Vikash Kumar © <https://orcid.org/0000-0002-3404-5180>
 Nitin Sharma © <https://orcid.org/0000-0001-9390-7127>
 Lokesh Srivastava © <https://orcid.org/0000-0003-0528-4295>
 Subrata Kumar Panda © <https://orcid.org/0000-0001-8841-7449>

References

1. H. S. Türkmen, Structural response of laminated composite shells subjected to blast loading: Comparison of experimental and theoretical methods, *J. Sound Vib.* **249** (2002) 663–678.
2. M. K. Yeh and Y. T. Kuo, Dynamic instability of composite beams under parametric excitation, *Compos. Sci. Technol.* **64** (2004) 1885–1893.
3. L. U. Chun and K. Y. Lam, Dynamic response of fully-clamped laminated composite plates subjected to low-velocity impact of a mass, *Int. J. Solids Struct.* **35** (1998) 963–979.
4. A. Gangwar, A. K. Sahu, V. Kumar, N. Sharma, M. Yavuz and S. K. Panda, Dynamic instability behaviour prediction of curved shell composite structure using different higher-order theories, *J. Vib. Eng. Technol.* **12** (2024) 8801–8814.
5. B. L. Wardle, P. A. Lagace and M. A. Tadele, Buckling response of transversely loaded composite shells, part 2: Numerical analysis, *ATAJ J.* **42** (2004) 1465–1473.
6. M. Ye, Y. Sun, W. Zhang, X. Zhan and Q. Ding, Nonlinear oscillations and chaotic dynamics of an antisymmetric cross-ply laminated composite rectangular thin plate under parametric excitation, *J. Sound Vib.* **287** (2005) 723–758.
7. M. Ye, J. Lu, W. Zhang and Q. Ding, Local and global nonlinear dynamics of a parametrically excited rectangular symmetric cross-ply laminated composite plate, *Chaos Solitons Fractals* **26** (2005) 195–213.
8. W. Zhang, C. Song and M. Ye, Further studies on nonlinear oscillations and chaos of a symmetric cross-ply laminated thin plate under parametric excitation, *Int. J. Bifurc. Chaos* **16** (2006) 325–347.
9. W. R. Chen, C. S. Chen and J. H. Shyu, Stability of parametric vibrations of laminated composite plates, *Appl. Math. Comput.* **223** (2013) 127–138.
10. S. Chakraborty, T. Dey and R. Kumar, Instability characteristics of damped CNT reinforced laminated shell panels subjected to in-plane excitations and thermal loading, *Structures* **34** (2021) 2936–2949.
11. S. Pradyumna and A. Gupta, Dynamic stability of laminated composite plates with piezoelectric layers subjected to periodic in-plane load, *Int. J. Struct. Stab. Dyn.* **11** (2011) 297–311.

- Collected Technical Papers (American Institute of Aeronautics and Astronautics, 1993), pp. 2261–2269.
30. A. Ghosh and P. K. Sinha, Dynamic and impact response of damaged laminated composite plates, *Aviat. Eng. Aerosp. Technol.* **76** (2004) 29–37.
 31. G. Serhat and I. Basdogan, Design of curved composite panels for optimal dynamic response using lamination parameters, *Compos. Part B* **147** (2018) 135–146.
 32. Y. Liu, Z. Qiu and F. Chu, Investigation of magneto-electro-thermo-mechanical loads on nonlinear forced vibrations of composite cylindrical shells, *Commun. Nonlinear Sci. Numer. Simul.* **107** (2022) 106146.
 33. B. Zhu, Y. Liu, N. Hojji, Z. Qiu and F. Chu, Vibration attenuation of rotating disks via acoustic black holes, *Int. J. Mech. Sci.* **242** (2023) 108025.
 34. E. Sohlani, A. R. Masoudi, Ö. Civalek and A. R. Ahmadi-Pari, Agglomerated impact of CNT vs. GNP nanofillers on hybridization of polymer matrix for vibration of conical hemispherical-conical conical shells, *Aerosp. Sci. Technol.* **120** (2022) 107257.
 35. M. H. Jabbari, H. T. Thai and Civalek, On viscoelastic transient response of magnetically imperfect functionally graded nanobeams, *Int. J. Eng. Sci.* **172** (2022) 103629.
 36. Ö. Civalek, S. Dastjerdi and B. Akgöz, Buckling and free vibrations of CNT-reinforced cross-ply laminated composite plates, *Mech. Based Des. Struct. Mach.* **50** (2022) 1914–1931.
 37. Ö. Civalek and M. Avrat, Free vibration and buckling analyses of CNT reinforced laminated non-rectangular plates by discrete singular convolution method, *Eng. Comput.* **38** (2022) 489–521.
 38. B. Safaei, N. A. Almuied and A. M. Fattahi, Free vibration analysis of polyethylene/CNT plates, *Eur. Phys. J. Plus* **134** (2019) 271.
 39. Z. Al Mahmoud, B. Safaei, S. Salmami, M. Asmael, M. A. Shalhzad, Q. Zechan and Z. Qiu, *Implementation of Different Types of Meshfree Technique in Computational Solid Mechanics: A Comprehensive Review Across Nano, Micro, and Macro Scales* (Springer Netherlands, 2024).
 40. J. K. Chen, A. Perca and F. A. Allaladi, Layer effects on the dynamic response of laminated composites, *Compos. Eng.* **5** (1995) 1135–1147.
 41. W. Song, Y. Zhong and J. Xiang, Mechanical parameters identification for laminated composites based on the impulse excitation technique, *Compos. Struct.* **162** (2017) 255–260.
 42. T. Liu, W. Zhang, Y. Zheng, Y. F. Zhang and W. Zhao, Potential well evolution and metastable dynamics of bistable asymmetric laminated composite square shallow shell under external and parametric excitations, *Compos. Struct.* **280** (2022) 114936.
 43. H. Babaei, S. Zafari, A. Kaveh, E. Aeshid and Ö. Civalek, Dynamic response of advanced lightweight porous plates integrated with nanocomposite face sheets resting on elastic substrate, *Int. J. Struct. Stab. Dyn.* **25** (2025) 1–29.
 44. Z. Al Mahmoud, B. Safaei, S. Salmami, M. Asmael and A. R. Setoodeh, *Computational Linear and Nonlinear Free Vibration Analysis of Micro/Nanoscale Composite Plate-Type Structures With/Without Considering Size Dependency Effect: A Comprehensive Review* (Springer Netherlands, 2025).
 45. L. Chen, Y. Chen, Y. Fu, J. Xu, D. An, J. Li, M. Ren and R. Li, A finite integral transform-based generalized eigenvalue formulation for buckling of orthotropic rectangular plates with rotational restraints, *Int. J. Struct. Stab. Dyn.* **2650032** (2024) 1–23.
 46. A. Garg, W. Zheng, M. Avcar, M. O. Belarbi, R. Kiran, L. Li and R. Raman, Free vibration behaviour of curved Miura-folded bio-inspired helicoidal laminated

A. K. Saba et al.

- composite cylindrical shells using HSDT assisted by machine learning-based IGA. *Compos. Struct.* **357** (2025) 118933.
47. A. Garg, N. K. Shukla, M. Avram, M.-O. Belarbi, W. Zheng, R. Raman, R. Kiani and L. Li, Free vibration analysis of annular and flat plates with sinusoidal corrugations using isogeometric analysis and machine learning-based stiffness modelling. *Thin-Walled Struct.* **215** (2025) 113492.
 48. A. Garg, N. Fantuzzi, M. Avcar and L. Li, High-fidelity surrogate driven bi-refined IGA for free vibration analysis of laminated composite annular plates with radial and curved cracks. *Arch. Civ. Mech. Eng.* **25** (2025) 225.
 49. A. Tabak, B. Safaei, A. Memarzadeh, S. Arman and C. Kizilbas, An extensive review of piezoelectric energy-harvesting structures utilizing auxetic materials. *J. Vib. Eng. Technol.* **12** (2024) 3153–3192.
 50. Z. Al-Mahmoud, B. Safaei, M. Asmael, M. S. Kenevial, S. Salmami, S. Karimzadeh, T. C. Jen and D. Hui, Impact of process parameters on mechanical and microstructure properties of aluminum alloys and aluminum matrix composites processed by powder-based additive manufacturing. *J. Manuf. Process.* **146** (2025) 79–154.
 51. A. Memarzadeh, B. Safaei, A. Tabak, S. Salmami and C. Kizilers, Advancements in additive manufacturing of polymer matrix composites: A systematic review of techniques and properties. *Mater. Today Commun.* **36** (2023) 105449.
 52. M. Asmael, Z. Al-Mahmoud, S. Salmami and B. Safaei, Enhancing tensile strength, adhesive joining of CF/PEEK and microstructure properties of epoxy by Nd_2O_3 rare-earth nanoparticles reinforcement. *Mater. Today Commun.* **41** (2024) 110854.
 53. O. Civalek and M. H. Jabali, Shear buckling analysis of functionally graded (FG) carbon nanotube reinforced skew plates with different boundary conditions. *Aerosp. Sci. Technol.* **99** (2020) 105753.
 54. A. E. Aghasoleghi, B. Akgar and O. Civalek, Magneto-thermoelastic interactions in an unbounded orthotropic viscoelastic solid under the Hall current effect by the fourth-order Moore-Gibson-Thompson equation. *Comput. Math. with Appl.* **141** (2023) 102–115.
 55. N. A. Abdullah, E. Sulaeman and M. I. M. Ahmad, LCO flutter instability on oscillating superionic wing by means of linearised aerodynamic small disturbance theory. In *Structural Integrity Cases in Mechanical and Civil Engineering* (Springer, 2022), pp. 13–27.
 56. W. C. Tai and I. Y. Shen, Parametric resonances of a spinning cyclic symmetric rotor assembled to a flexible stationary housing via multiple bearings. *J. Vib. Acoust.* **135** (2013) 051030-1–051030-9.
 57. Y. Li, T. Chen and X. Wang, Non-linear dynamics of gear pair with dynamic backlash subjected to combined internal and external periodic excitations. *J. Vib. Control* **22** (2016) 1693–1703.
 58. C. K. Hirwani, R. K. Patil, S. K. Panda, S. S. Mahapatra, S. K. Mandal, L. Srivastava and M. K. Buragohain, Experimental and numerical analysis of free vibration of delaminated curved panel. *Aerosp. Sci. Technol.* **54** (2016) 353–370.
 59. V. K. Singh and S. K. Panda, Nonlinear free vibration analysis of single/doubly curved composite shallow shell panels. *Thin-Walled Struct.* **85** (2014) 341–349.
 60. B. Adhikari and B. N. Singh, Parametric instability analysis of laminated composite plate subject to various types of non-uniform periodic in-plane edge load. *Appl. Math. Comput.* **373** (2020) 125026.